Image Aesthetic Reasoning via HCM-GRPO: Empowering Compact Model for Superior Performance

Zhiyuan Hu^{a,*,1}, Zheng Sun^{b,*,†}, Yi Wei^b, Long Yu^{b,†}

^aTsinghua University, Beijing, 100084, China

^bAlibaba Health Information Technology Limited, Beijing, 100102, China

Abstract

The performance of image generation has been significantly improved in recent years. However, the study of image screening is rare and its performance with Multimodal Large Language Models (MLLMs) is unsatisfactory due to the lack of data and the weak image aesthetic reasoning ability in MLLMs. In this work, we propose a complete solution to address these problems in terms of data and methodology. For data, we collect a comprehensive image screening dataset with over 128k samples, about 640k images. Each sample consists of an original image, four generated images. The dataset evaluates the image aesthetic reasoning ability under four aspects: appearance deformation, physical shadow, placement layout, and extension rationality. Regarding data annotation, we investigate multiple approaches, including purely manual, fully automated, and answer-driven annotations, to acquire high-quality chains of thought (CoT) data in the most cost-effective manner. Methodologically, we introduce a Hard Cases Mining (HCM) strategy with a Dynamic Proportional Accuracy (DPA) reward into the Group Relative Policy Optimization (GRPO) framework, called HCM-GRPO. This enhanced method demonstrates superior image aesthetic reasoning capabilities compared to the original GRPO. Our experimental results reveal that even state-of-theart closed-source MLLMs, such as GPT40 and Qwen-VL-Max, exhibit performance akin to random guessing in image aesthetic reasoning. In contrast, by leveraging the HCM-GRPO, we are able to surpass the scores of both large-scale open-source and leading closed-source models with a much smaller model.

Keywords: Multimodal large language models, image aesthetic reasoning, reinforcement learning

1. Introduction

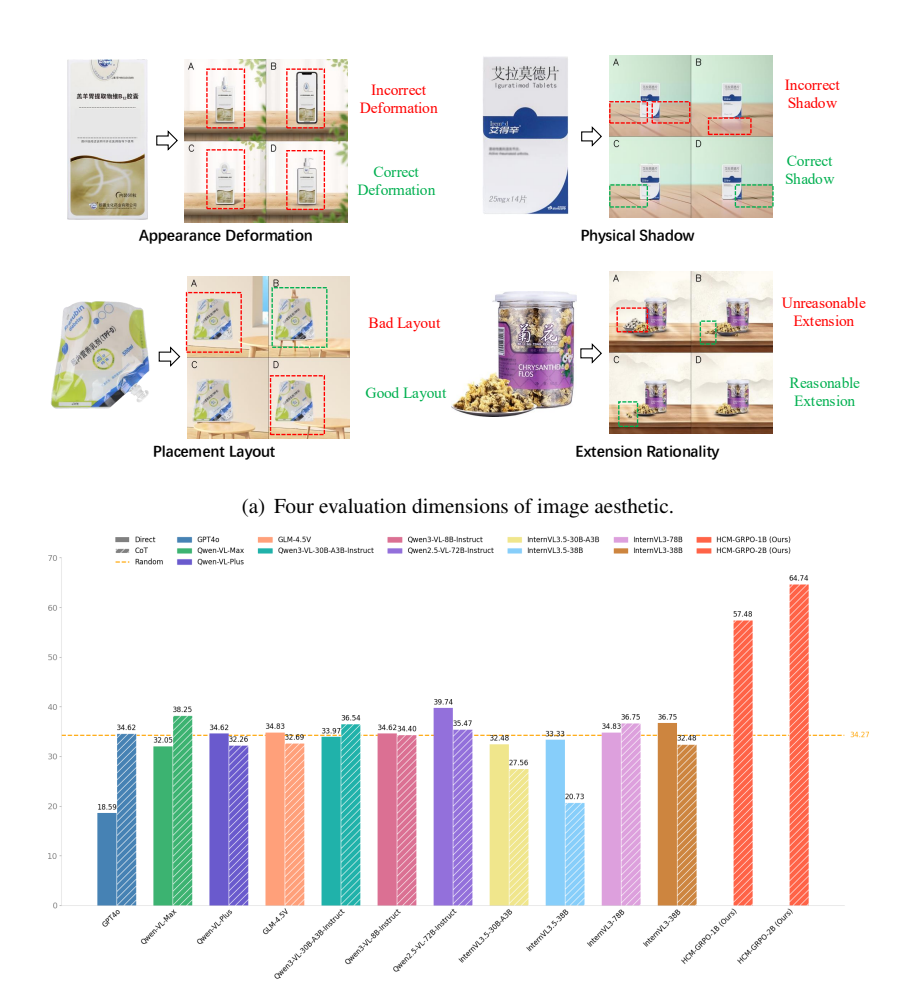
In recent years, there have been extensive researches on Multimodal Large Language Models (MLLMs), covering foundational model development [1, 2, 3], evaluation dataset construction [4, 5, 6], reinforcement learning (RL) applications [7, 8, 9], and even areas related to AI-Generated Content (AIGC) [10, 11, 12, 13]. At the same time, thanks to the development of diffusion models [14, 15, 16, 17, 18] and unified MLLMs [13, 19], the performance of image generation has also been greatly improved. The diffusion process of images involves a certain degree of randomness, so it often requires specific conditions to provide directed control [20]. However, even with constraints on the generation process, the model may still produce some unpredictable results. Therefore, it is highly necessary to conduct a screening process for the generated images. MLLMs are capable of processing information from different modalities, such as text, image and video, simultaneously, and providing responses based on a comprehensive understanding. Against this background, this paper focuses on exploring the image aesthetic reasoning ability of MLLMs.

Image aesthetic reasoning with MLLMs is hindered by the scarcity of specialized datasets and the suboptimal reasoning abilities of existing models. In response, advancements have been achieved through the development of a novel dataset and an advanced approach. The collected dataset in this paper consists of over 128k samples, providing indispensable knowledge for model training. In contrast to prior studies [21, 22, 23, 24], our dataset places significant emphasis on the physical space transformations of AI-generated images. These transformations are straightforward to eval-

^{*}Equal contribution.

[†]Corresponding author.

¹Work done when Zhiyuan Hu was an intern at Alibaba Health Information Technology Limited, Beijing, China.



(b) Quantitative comparison results.

Figure 1: Overview of the image aesthetic dataset and quantitative comparison results. (a) We summarize four evaluation dimensions of image aesthetic from the dataset. (b) Extensive quantitative comparison results demonstrate the superiority of our HCM-GRPO method in the image screening task.

uate objectively, avoiding any reliance on subjective artistic criteria. The generated images consist of the foreground medicines, backgrounds, and layout settings. All the medicines are derived from the real-world. We randomly select a background image from the background image set and randomly assign a layout (either top-bottom or left-right) for the original medicine image. Then, we use a segmentation model [25] on the original image to obtain the mask of the foreground. Based on the assigned

layout region, we determine the position of the foreground target. Finally, we use an image generation model [26] to render the areas outside the foreground medicine, referencing the selected background image. In the generated images, we observe a significant amount of unintended content due to randomness. As shown in Figure 1 (a), we categorize these issues into four types: appearance deformation, physical shadow, placement layout, and extension rationality. We summarize the ability to identify these four types of issues as image aesthetic reasoning capability. After collecting the images, we assign the four generated images the labels A, B, C, and D, and manually annotate the correct images in the form of multiple-choice answers in the training and testing datasets, such as "AC", "BCD", or "N". We test various state-of-the-art closed-source and open-source MLLMs for the identification of problematic images, with the final results presented in Figure 1 (b). From the results, we conclude that directly using existing models yields very poor performance, with scores on our testing dataset being nearly equivalent to random guessing. Based on this, we further propose a two-stage approach to enhance the image aesthetic reasoning capability of smallsized MLLMs. Specifically, in the first stage, we investigate multiple approaches to acquire chains of thought (CoT) data to perform supervised fine-tuning (SFT) on the base model to adapt it to the specific response format. Purely manual annotation produces the highest quality CoT data but incurs high associated costs and a slow pace, making it difficult to scale. Fully automated annotation is extremely low-cost and highly scalable. However, it sacrifices quality, often generating noisy data that contains factual errors or hallucinations. Answer-driven annotation serves as a strategic trade-off. It leverages the final answer from humans and the thought process from existing models to accelerate the process and reduce costs. It balances the efficiency of automation with the reliability of human expertise. In the second stage, we propose Hard Cases Mining (HCM) in Group Relative Policy Optimization (GRPO) [27, 28] with Dynamic Proportional Accuracy (DPA) reward, called HCM-GRPO, to stimulate the model's reasoning ability. The HCM-GRPO first utilizes an initial model to partition the dataset into easy and hard cases, then it strategically focuses on these hard cases during the latter stage of training through hard cases mining. Concurrently, the integrated DPA reward provides a significantly denser reward signal to guide the optimization process more effectively. Ultimately, our approach achieves a score of 64.74 on the evaluation dataset with InternVL3-2B, surpassing large-sized open-source and leading closed-source models. Moreover, our experimental results on public datasets validate the applicability of HCM-GRPO to real-world and multi-image understanding tasks. The main contributions of this paper can be summarized as follows:

- We develop a pipeline for image fusion and generation, curating an image screening dataset with more than 640k images, which is specifically designed for training and testing MLLMs, as well as for the proposed method for image aesthetic reasoning. Our dataset is built upon authentic, real-world images of medicinal products.
- We present a two-stage approach, which includes a scalable methodology for acquiring high-quality CoT data and an enhanced, more effective reinforcement learning method, HCM-GRPO. This methodology achieves a significant enhancement compared to the performance of the base model. The small model HCM-GRPO-2B surpasses both large-sized open-source and closed-source models by over 20 points on the scoring metric.
- We conduct extensive experiments on established and other public benchmarks. The experimental results reveal that current MLLMs still have significant deficiencies in understanding image aesthetic and our HCM-GRPO can effectively enhance the performance of the base model. It is hoped that this work will provide a valuable reference for research in the MLLMs and AIGC communities.

2. Related Work

2.1. Multimodal Large Language Models

MLLMs have demonstrated impressive capabilities across various tasks and applications [1, 3, 7, 29, 30, 31]. Particularly, an increasing number of studies are exploring the scope and boundary of MLLMs' capabilities. For instance, CC-OCR [5] investigates the performance of MLLMs on end-to-end OCR tasks. Naturalbench [32]

examines their ability to understand when faced with the same question under different images. CoMT [6] explores their visualization capabilities during the reasoning process. All-Angle Bench [33] studies MLLMs' multi-perspective understanding and corresponding abilities. Inspired by the frequent occurrence of unreasonable content in the field of image generation, we are very curious about whether MLLMs can understand human preferences regarding the generated content. In this work, we construct a pipeline for the image generation dataset and evaluate the performance of various MLLMs based on this dataset.

2.2. Reinforcement Learning

Recently, reinforcement learning techniques have been extensively applied to enhance the reasoning capabilities of Large Language Models (LLMs), enabling them to effectively solve complex problems [27, 28, 34, 35, 36, 37]. Deepseek-R1 [28] is a milestone work in the application of reinforcement learning to the domain of LLMs. It includes the full version of DeepSeek-R1 and DeepSeek-R1-Zero, which are obtained using Group Relative Policy Optimization (GRPO). Based on GRPO, DAPO [34] introduces several key techniques to make RL shine in the long-CoT RL scenario with Qwen2.5-32B, outperforming the DeepSeek-R1-Zero-Qwen-32B while using only half the training steps in AIME 2024. VAPO [35] proposes a novel framework tailored for reasoning models within the value model-based paradigm, pinpointing three key challenges that plague value model-based methods: value model bias, the presence of heterogeneous sequence lengths, and the sparsity of reward signals. As for MLLMs, RL is often applied to specific tasks, such as object detection [7], training reward models [38], and enhancing reasoning capabilities [39], which often require designing task-specific rewards. In this paper, we apply the reinforcement learning method GRPO to a new task: screening generated images with MLLMs. The proposed HCM-GRPO method, even when applied to small-sized models, outperforms both large-sized open-source and closed-source models.

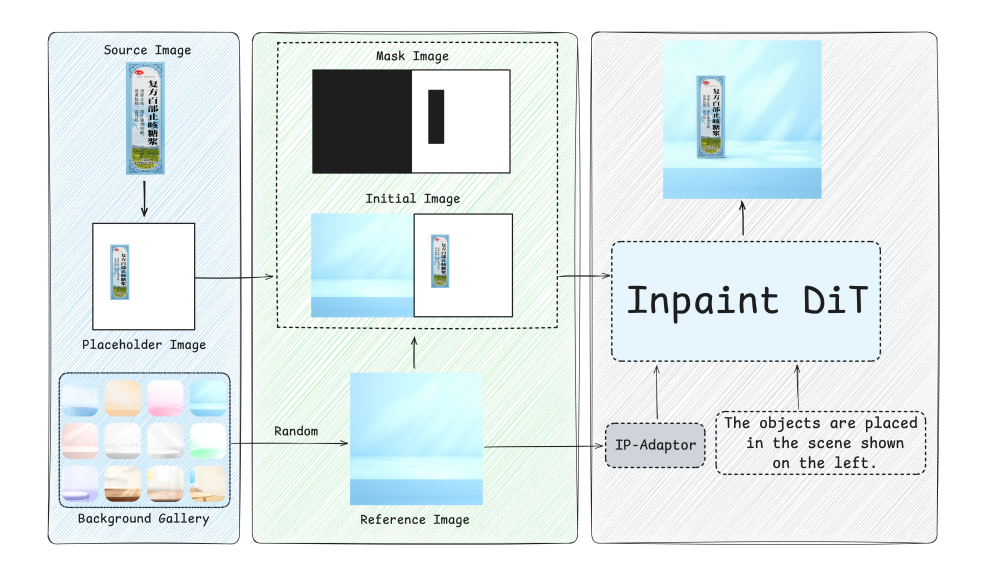


Figure 2: Overview of dataset construction pipeline.

3. Image Screening Dataset

3.1. Image Fusion and Generation

In this section, we mainly introduce the data construction pipeline and provide detailed information about the dataset. The construction process can be divided into three stages, as shown in Figure 2. The first stage is the data preparation phase. We first obtain source images of various medicines and use an open-source image segmentation model [25] to extract the foreground regions of the medicines. These regions are then placed onto a preset area of a white background image to create the placeholder image. Meanwhile, we randomly select a background image from the background gallery as the reference image. The second stage is the data processing phase. We combine the placeholder image and the reference image to create the initial image. Additionally, we generate a mask image based on the placeholder image. The mask image also consists of two parts: the left half is entirely black, while the right half is white, except for the target region. Notably, we attempt to use only the right half of the mask image and the initial image as input, however, the final rendering results are unsatisfactory. Therefore, both the initial image and the mask image include both the left and right halves. The third stage is the generation phase. Here, we utilize FLUX.1-Fill-dev and

Table 1: An overview of the different dataset splits, detailing their characteristics such as size, label accuracy, CoT data, and supervision type.

Dataset Split	Training	Testing	Pseudo-Label	Exploration
Size	1,044	468	10,724	115,809
Multiple-choice Label	\checkmark	\checkmark	×	×
CoT Data	✓	×	\checkmark	×
Supervision Type	Fully + Answer-driven	Fully	Weakly	Unsupervised

FLUX.1-Redux-dev [26] as Inpaint DiT [17] and IP-Adapter [18], respectively. The reference image is fed into the IP-Adapter to serve as a controller, while the mask image and the initial image are simultaneously input into the Inpaint DiT for repainting. In summary, the process involves redrawing the initial image with the white regions in the mask image by referencing the reference image.

Based on the pipeline described above, we collect over 640k images, which are ultimately grouped into more than 128k samples. The dataset contains over 56,500 types of medicines, more than 20 background images and 4 evaluation dimensions. As shown in Figure 1 (a), these four evaluation dimensions are as follows: (1) appearance deformation, which refers to differences in appearance between the generated image and the original medicine; (2) physical shadow, which indicates noticeable errors in lighting and shadow, such as inconsistent shadow directions among objects; (3) placement layout, which refers to unrealistic scenarios, such as floating objects in the image; (4) extension rationality, which involves the principle of generating logically consistent associations while strictly prohibiting fabrications that lack any grounding in the original medicine image. We summarize the ability to identify these four types of issues as image aesthetic reasoning capability. The most common issue during the image generation process is appearance deformation, and only a small portion (8.5%) of the images are normal. Excluding the normal part, we focus on evaluating the ability of MLLMs to recognize issues across the remaining four dimensions. More visualization examples can be found in Appendix A.

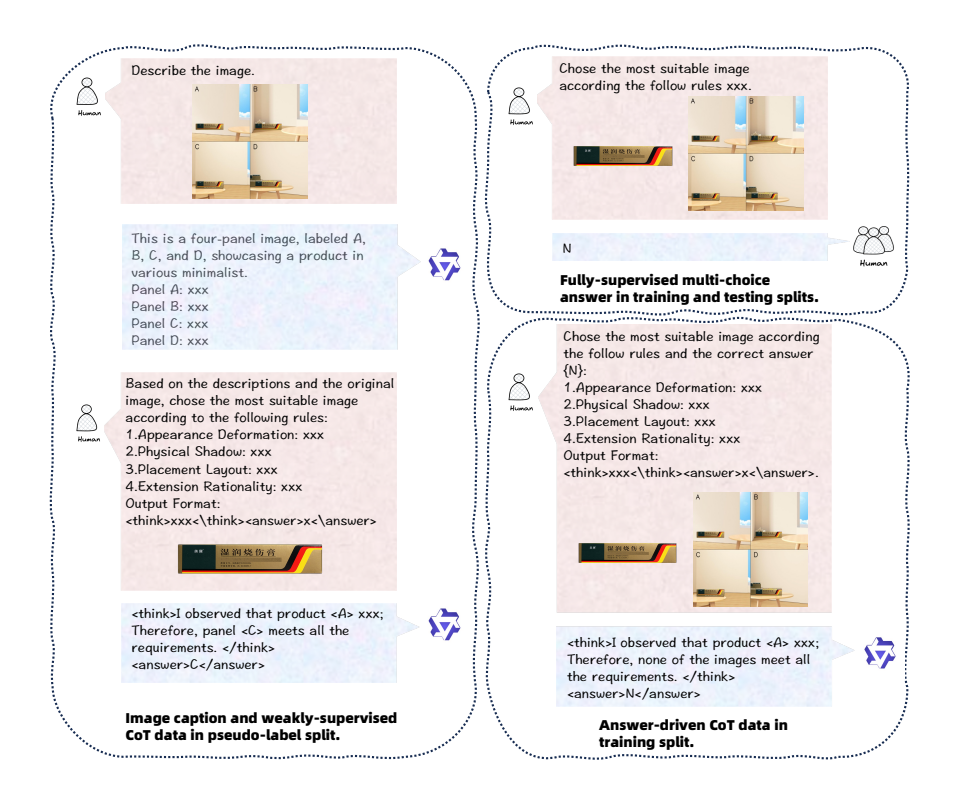


Figure 3: Presentation of different annotation paradigms.

3.2. Dataset Division and Annotation

As shown in Table 1, our dataset is divided into training, testing, pseudo-label, and exploration splits, comprising a total of 128k unique samples. Each sample includes an original medicine image and four generated images.

In the training and testing splits, manual annotation is performed by human reviewers to ensure ground-truth accuracy, as shown in the top-right part of Figure 3. Samples in the training set are labeled with the ground-truth multiple-choice answer, which may contain several correct options, such as "ACD", "BC", or "N". Samples in the testing set contain multiple-choice labels for overall evaluation and dedicated evaluation dimension types. This latter annotation allows for a nuanced assessment of the model's capabilities in perceiving different aesthetic dimensions of the images. The annotation process is exceptionally time-consuming, as it requires a detailed inspection of the four optional images for each sample.

Furthermore, annotating CoT data would be even more laborious, as it involves documenting the reasoning process across four distinct aesthetic dimensions for each of the four options. Given this prohibitive complexity, we leverage the Qwen-VL-Max [40] model for automated labeling to enhance the diversity and richness of the descriptive tags in the pseudo-label split. We design a progressive annotation paradigm to enable the model to generate accurate image descriptions and structured reasoning processes. As shown in the left part of Figure 3, for each sample in our pseudo-label split, we first prompt the model to describe what it sees in the image. Since image captioning is a fundamental and common task during the pre-training of MLLMs, we operate under the assumption that the model can generate these basic descriptions with high accuracy. Then, the model is instructed to integrate its own description, structure its reasoning process, and conclude with the final answer. Consequently, within our pseudo-label split, we generate two distinct types of pseudo-labeled data: one is the image description, and the other is the CoT data grounded in this description.

For the final exploration split, we generate four synthetic images from each original image but provide no annotations. This portion of the data is intentionally left unlabeled to serve as a testbed for future exploration of unsupervised methods.

4. Method

4.1. Cold Start: Basic Spatial Understanding and Instruction Following

We expect MLLMs to possess basic capabilities in the image aesthetic reasoning task, such as instruction-following and fundamental spatial change recognition. However, the training data for these MLLMs often fails to cover specific scenarios. This limitation results in the base model being unable to output responses in a specific format as instructed, and the generated content often contains hallucinations. As a result, direct application of reinforcement learning methods tends to incur significant consumption of training resources, while the final outcomes still fall short of optimality. Inspired by DeepSeek-R1-Zero and DeepSeek-R1 [28], we perform cold-start training using CoT data before the reinforcement learning phase.

This process involves acquiring CoT data, which is resource-intensive for the image

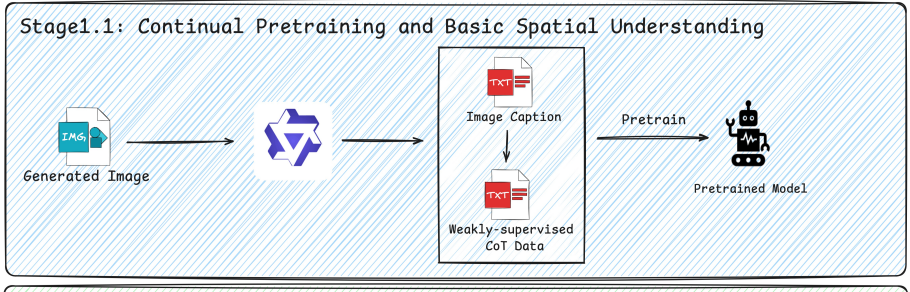
screening task, as it requires annotators to carefully examine the details of each image. To address this issue, we design two distinct methods for acquiring CoT data. The first method is described in our pseudo-label split, which involves generating an image description followed by the corresponding reasoning steps. Although the accuracy of these weakly-supervised CoT data is relatively modest with an approximate accuracy of 38.25% (as indicated in Table 3), our primary focus lies not in the absolute accuracy of the data. Instead, we aim to determine whether this data can enable the model to respond in a fixed format and develop basic spatial change recognition abilities. In our second method, we recognize that the core value of CoT data lies in the reasoning process. Allowing Owen-VL-Max to directly generate this process would be equivalent to unconstrained self-generation, lacking proper guidance. Therefore, we leverage samples from the training set, conditioning on the human-annotated correct answers, to prompt Qwen-VL-Max to regenerate 1,044 answer-driven CoT data samples. This procedure is illustrated in the bottom-right part of Figure 3. In our training process, these two methods for generating CoT data are applied sequentially. We first perform continual pretraining and basic spatial understanding on the image caption and weaklysupervised CoT data, followed by answer-driven spatial understanding and instruction following on the answer-driven CoT data. This training pipeline is illustrated in Figure 4 Stage 1.1 and Stage 1.2. The objective function of SFT is defined as:

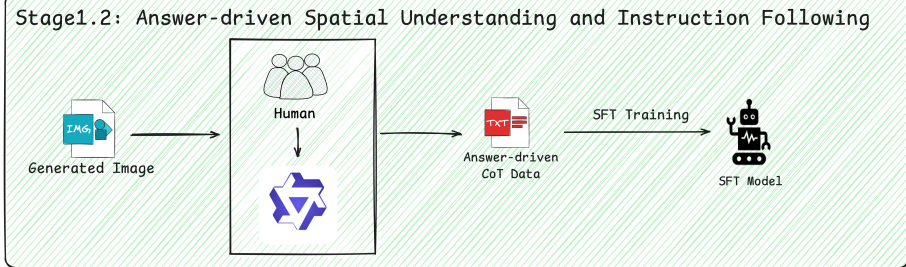
$$\mathcal{L}_{cold_start}(\theta) = -\sum_{i=1}^{T} \log p(y_i|x, y_{< i}; \theta), \tag{1}$$

where x is the original input, $y = \{y_1, y_2, ..., y_T\}$ is the distilled output from Qwen-VL-Max, and θ represents the parameters of the base model. This stage serves to initialize the model's ability to follow a structured CoT reasoning format.

4.2. HCM-GRPO: Reinforcement Fine-Tuning and Hard Cases Mining

GRPO foregoes the critic model that is typically the same size as the policy model, and estimates the baseline from group scores instead [28]. Given an input q, GRPO first samples G distinct responses $\{o_i\}_{i=1}^G$ from the old policy model π_{old} . Each response is evaluated by the pre-designed reward functions, i.e., format and accuracy, to calculate the corresponding reward scores $\{r_i\}_{i=1}^G$. Then, GRPO computes the difference between





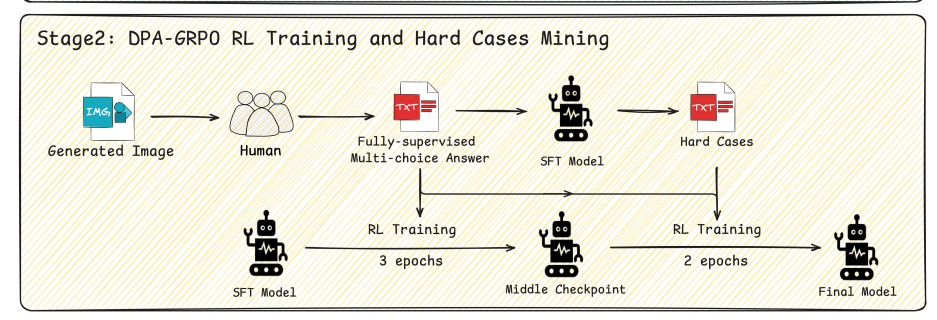


Figure 4: Illustration of model training process.

each reward and the mean of the reward score group, which can be regarded as the baseline value, and normalizes the differences using the standard deviation:

$$A_i = \frac{r_i - mean(\{r_1, r_2, ..., r_G\})}{std(\{r_1, r_2, ..., r_G\})},$$
(2)

where A_i quantifies the relative quality of the *i*-th response in comparison to other candidates within the same sampled group. Based on the simple advantage A_i , GRPO optimizes the policy model π_{θ} by maximizing the following objective:

$$\mathcal{J}_{GRPO}(\theta) = \mathbb{E}[q \sim P(Q), \{o_i\}_{i=1}^G \sim \pi_{old}(O|q)]$$

$$\frac{1}{G} \sum_{i=1}^G (\min(w_i A_i, clip(w_i, 1 - \epsilon, 1 + \epsilon) A_i) - \beta \mathbb{D}_{KL}(\pi_{\theta} || \pi_{ref})),$$
(3)

$$\mathbb{D}_{KL}(\pi_{\theta}||\pi_{ref}) = \frac{\pi_{ref}(o_i|q)}{\pi_{\theta}(o_i|q)} - \log \frac{\pi_{ref}(o_i|q)}{\pi_{\theta}(o_i|q)} - 1,$$
(4)

$$w_i = \frac{\pi_{\theta}(o_i|q)}{\pi_{old}(o_i|q)},\tag{5}$$

where w_i is the importance sampling coefficient, β is a hyper-parameter that avoids the policy model from diverging too far from the reference model π_{ref} . ϵ clips the extreme importance sampling coefficient for stability.

In Deepseek-R1 [28], the overall verifiable reward *r* is formulated as:

$$r = r_{fmt} + r_{acc},\tag{6}$$

where r_{fmt} and r_{acc} stand for format reward and accuracy reward, respectively. The format reward encourages the model's responses to follow a fixed structure, including <think></think><answer></answer>. In this paper, we retain this reward by using prompts, provided in Appendix B, to guide the model to output responses in a fixed format. Additionally, the role of first-stage CoT learning is to ensure that the model can stably generate responses in this specific format.

The accuracy reward evaluates whether the final answer exactly matches the ground truth. Our HCM-GRPO differs from the original GRPO primarily in two aspects: the design of the reward function and the training paradigm. In the task of image aesthetic reasoning, we believe that the design of the accuracy reward for multiple-choice questions is crucial. Since a sample may have multiple correct options, we treat the multiple-choice answer as a complete answer and introduce a Dynamic Proportional Accuracy (DPA) reward. Under this schema, the accuracy reward value is no longer binary, it is tied to the length of the multiple-choice answer instead:

$$r_{acc} = \begin{cases} \frac{len(response)}{len(answer)}, & if \ response \ in \ answer \\ 0, & otherwise \end{cases}$$
 (7)

The rationale behind this design is that the reward function should measure the gap between the response and the correct answer as accurately as possible. When humans solve a multiple-choice question, a score of 0 should be given if the response is incorrect. However, if the response is part of the correct answer, partial credit should be

awarded, with a score between 0 and 1. A full reward, such as 1, is given only when the response is completely correct. We term GRPO with DPA reward as DPA-GRPO. To further enhance the model's sophisticated reasoning abilities beyond the initial supervised fine-tuning, we introduce an advanced reinforcement learning strategy termed Hard Cases Mining in Group Relative Policy Optimization (HCM-GRPO). As illustrated in Figure 4 Stage2, this method is designed to compel the model to learn from its mistakes by focusing on challenging examples. The process begins with a hard case identification step, where we leverage the SFT model from Stage1 to evaluate the entire training set against the human-annotated, fully-supervised multiple-choice answers. Samples answered correctly are classified as easy cases, while those answered incorrectly are designated as hard cases. This curated set of hard cases is then integrated into a specialized RL training schedule using the DPA-GRPO algorithm. For the first 3 epochs, the model undergoes general training on the complete dataset to establish a robust baseline. Subsequently, in the final 2 epochs, we implement the hard cases mining strategy by augmenting the training data, re-introducing the identified hard cases alongside the full dataset. This oversampling of challenging examples compels the model to dedicate more learning capacity to its weaknesses, thereby refining its reasoning pathways and leading to a more capable final model.

5. Experimental Result

5.1. Experimental Setting

We conduct experiments on the collected image screening dataset for the task of image aesthetic reasoning. Furthermore, we validate its performance on several public datasets to assess its capabilities in real-world spatial reasoning and multi-image understanding. Our HCM-GRPO demonstrates competitive performance by utilizing hard cases mining in GRPO compared to others.

Baseline Models. For the baseline models used for cross-sectional comparison, we select several large-sized open-source models, such as InternVL3.5-30B-A3B [41], InternVL3-78B [1], Qwen2.5-VL-72B-Instruct [2] and GLM-4.5V [31], as well as some closed-source models like GPT4o [42], Qwen-VL-MAX [40], and Qwen-VL-

Table 2: Training parameters.

Parameter	SFT	GRPO (DPA-GRPO)	HCM-GRPO
Freeze LLM	False	False	False
Freeze ViT	True	False	False
Freeze Aligner	True	False	False
Epochs	5	5	3+2
Per-device Batch Size	8	8	8
G for Group Generations	NULL	4	4
β for KL divergence	NULL	0.04	0.04
Top_k	NULL	3	3
Top_p	NULL	0.8	0.8
Temperature	NULL	1	1

Plus [43]. For the baseline compact models used for longitudinal comparison, we select InternVL3-1B and InternVL3-2B [1] to validate the effectiveness of our proposed HCM-GRPO.

Hyperparameter Settings. All experiments are implemented via trl based on the training framework SWIFT [44], a flexible and efficient tool for supervised fine-tuning and reinforcement learning. As shown in Table 2, we compare several distinct training paradigms. In SFT, the Vision Transformer (ViT) and Aligner of MLLMs are frozen, with no generative sampling strategies, focusing on structured supervised learning with a batch size of 8. In contrast, GRPO unfreezes all components and introduces advanced generative sampling techniques, including $Top_k = 3$, $Top_p = 0.8$, and Temperature = 1, enabling stochasticity during training. Additionally, GRPO incorporates a KL divergence penalty with a β coefficient of 0.04 to balance exploration and stability, while SFT omits this term entirely. Despite sharing common settings, such as 5 training epochs, the two paradigms differ significantly in their designs. GRPO highlights its adaptability for complex tasks, whereas SFT emphasizes simplicity and stability.

Evaluation Metrics. Due to the high difficulty of the image aesthetic reasoning task, we differentiate the evaluation metric from the dynamic proportional accuracy reward. Specifically, if the model's response is among the correct options in a multiple-choice question, we consider it correct. Our model is designed for a real-world e-commerce task: product image screening. In this scenario, only one image is ultimately displayed on the webpage. Therefore, if the model suggests multiple valid images, we would simply select one from its recommendations. As long as the model provides one correct option, the task is successfully completed, provided that all the output options of the model are correct. In this way, there is no need to identify all the correct options. **Random Guessing.** The random guessing baseline score of 34.27 is a calculated expectation rather than an empirical result from a random simulation. It is derived from the specific structure of our test set, where each sample can have one or more correct options. Through statistical analysis of the test set, we determine that the average length of correct options per sample is 1.7136. Since a guess involves picking one from five choices (A, B, C, D, N), the expected probability of success is 1.7136 divided by 5, which equals 0.3427.

5.2. Comparison with Prior Arts

We compare our proposed HCM-GRPO method on small models with several open-source large-sized and closed-source MLLMs. During evaluation, we assess the performance of both direct and CoT format prompts, reporting the overall score as well as the scores for the four evaluation dimensions. The results are shown in Table 3. In general, all models exhibit suboptimal performance on our dataset, with scores approximately equivalent to that of random guessing. This indicates that these models lack image aesthetic reasoning capabilities. Among these compared models, the best-performing one is Qwen2.5-VL-72B-Instruct.

For our own HCM-GRPO models, HCM-GRPO-2B achieves substantial improvements across most dimensions, particularly in appearance deformation and extension rationality. However, it still struggles with recognizing more advanced physical rules, such as placement layout. The experimental results align with human-like recognition abili-

Table 3: Comparison results. We evaluate the image screening performance of both closed-source and open-source MLLMs. We use bold to highlight the top results, and underline to indicate the second-best results. Notably, the overall score includes four dimensions of image aesthetic ability and the normal type.

Models	Prompt	Overall	Appearance	Physical	Placement	Extension
Models	Type	Score	Deformation	Shadow	Layout	Rationality
Random	-	34.27	27.61	31.46	29.49	27.25
		API-bas	ed models			
GPT4o	Direct	18.59	18.66	13.41	22.88	20.59
GP140	CoT	34.62	23.51	29.27	24.58	29.41
Owen VI. Man	Direct	32.05	21.64	26.83	25.42	15.67
Qwen-VL-Max	CoT	38.25	29.10	37.80	25.42	28.43
Owen VI Plea	Direct	34.62	22.76	35.37	25.42	27.45
Qwen-VL-Plus	CoT	32.26	21.27	29.27	25.42	28.43
		Open-sou	rce MLLMs			
CLM 45W	Direct	34.83	23.88	29.27	27.97	26.47
GLM-4.5V	CoT	32.69	20.90	30.49	22.03	23.53
0 2 14 200 120 1	Direct	33.97	23.51	25.61	25.42	26.47
Qwen3-VL-30B-A3B-Instruct	CoT	36.54	27.99	36.59	22.88	30.39
0 214 001	Direct	34.62	23.88	32.93	24.58	24.51
Qwen3-VL-8B-Instruct	CoT	34.40	21.64	29.27	25.42	24.51
0 05 111 700 1	Direct	39.74	29.85	40.24	32.20	30.39
Qwen2.5-VL-72B-Instruct	CoT	35.47	25.00	35.37	25.42	25.49
1 . MA 5 20D A2D	Direct	32.48	20.90	26.83	22.03	26.47
InternVL3.5-30B-A3B	CoT	27.56	18.28	21.95	22.03	25.49
Y . Y . Z . Z . 20D	Direct	33.33	20.90	26.83	25.42	25.49
InternVL3.5-38B	CoT	20.73	13.06	21.95	13.56	15.69
1 . VII 2 70D	Direct	34.83	23.88	31.71	24.58	27.45
InternVL3-78B	CoT	36.75	26.49	31.71	29.66	28.43
L.,	Direct	36.75	26.49	32.93	30.51	27.45
InternVL3-38B	CoT	32.48	21.27	24.39	24.58	26.47
HCM-GRPO-1B (Ours)	СоТ	57.48	58.21	60.98	62.71	57.84
HCM-GRPO-2B (Ours)	CoT	64.74	68.66	65.85	<u>55.08</u>	74.51

ties: changes in appearance and quantity are indeed easier to comprehend compared to physical layout and shadow.

Table 4: Comparison between direct answering and reasoning.

Models	Prompt Type	Overall Score	
InternVL3-1B	Direct	30.13	
International	CoT	25.85	
+SFT	Direct	36.75	
+GRPO	СоТ	28.42	
InternVL3-2B	Direct	10.68	
Intern V L3-2B	CoT	23.72	
+SFT	Direct	45.94	
+GRPO	СоТ	28.42	

5.3. Ablation Studies

We conduct a series of experiments to evaluate the effectiveness of different modules in our approach based on InternVL3-1B and InternVL3-2B.

Comparison Between Direct Answering and Reasoning. By utilizing the training set, we first compare the original models, the original models fine-tuned with direct answers, and the original models enhanced with GRPO. As shown in Table 4, the models fine-tuned directly with answers achieve the highest scores of 36.75 and 45.94. However, applying GRPO directly on the source models proves to be completely ineffective. After applying GRPO to InternVL3-1B and InternVL3-2B, we find that the models acquire the same score. This phenomenon may be attributed to the fact that the original models lack sufficient instruction-following and basic spatial understanding capabilities, thereby leading to the failure of the accuracy-based reward.

Effectiveness of Different Sources of CoT Data. The results in Table 4 indicate that directly fine-tuning the model with answers yields limited improvements, and that RL-based methods like GRPO are ineffective when applied to the base model. This motivates us to first develop a base model with foundational reasoning capabilities. To this end, we utilize the previously acquired CoT data: image captions and weakly-supervised CoT data generated by Qwen-VL-Max on the pseudo-label split,

Table 5: Effectiveness of different CoT data with InternVL3-1B and InternVL3-2B

Ехр	Image Caption Data	Weakly-supervised CoT Data	Answer-driven CoT Data	Overall Score
InternVL3-1B				25.85
Exp1	×	✓	×	34.19 (+8.34)
Exp2	✓	✓	×	34.62 (+8.77)
Exp3	×	×	✓	39.96 (+14.11)
Exp4	\checkmark	✓	\checkmark	45.94 (+20.09)
InternVL3-2B				23.72
Exp1	×	✓	×	34.83 (+11.11)
Exp2	\checkmark	\checkmark	×	35.04 (+11.32)
Exp3	×	×	✓	51.07 (+27.35)
Exp4	✓	✓	\checkmark	53.63 (+29.91)

as well as the human-annotated, answer-driven CoT data generated on the training set. We then conduct a systematic ablation study to determine the most effective CoT data acquisition method in Table 5. This process also allows us to explore the performance ceiling of a cold-start approach, ultimately resulting in a base model equipped with proficient reasoning skills. Taking InternVL3-2B as an example, the comparison among InternVL3-2B, Exp1, and Exp2 highlights the impact of incorporating weakly-supervised CoT data and image caption data. The introduction of weaklysupervised CoT data alone (Exp1) yields a substantial performance gain over the baseline InternVL3-2B model. The overall score increases from 23.72 to 34.83, a significant improvement of 11.11 points. This demonstrates that even without groundtruth guidance, training on auto-generated reasoning steps provides a basic foundation for improving the model's capabilities. Further augmenting the training set with image caption data (Exp2) on top of the weakly-supervised CoT data results in only a marginal improvement, increasing the score from 34.83 to 35.04. This suggests that while image captions are slightly beneficial, their contribution is minimal compared to the primary impact of the CoT data in this experimental setup. The comparison between Exp2 and Exp3 reveals a critical finding regarding the quality of CoT data. A

Table 6: Comparison among different GRPO paradigms.

Models	Overall Score
InternVL3-1B-CoT	45.94
+GRPO	53.85 (+7.91)
+DPA-GRPO	55.56 (+9.62)
+HCM-GRPO	57.48 (+11.54)
InternVL3-2B-CoT	53.63
+GRPO	58.55 (+4.92)
+DPA-GRPO	59.83 (+6.20)
+HCM-GRPO	64.74 (+11.11)

striking disparity in effectiveness is observed when comparing Exp2 and Exp3. By exclusively using answer-driven CoT data (Exp3), the model's overall score dramatically increases to 51.07. This score is 16.03 points higher than 35.04 of Exp2. This result strongly indicates that high-quality CoT data, generated with the guidance of human-annotated answers, is significantly more effective at enhancing the model's reasoning performance than its weakly-supervised counterpart. Furthermore, Exp4 represents the model trained with all available data sources and establishes the upper bound of SFT performance in our experiments. By integrating all three types of data, Exp4 achieves the highest score of 53.63. This is a notable improvement of 2.56 points over using only the most effective single data source, answer-driven CoT data. This suggests a synergistic effect, where the high-quality, answer-driven CoT data is complemented by the broader contextual understanding from image captions and the diverse reasoning patterns from weakly-supervised data, leading to the best overall performance. This conclusion is also supported by our experiments on InternVL3-1B.

Comparison among Different GRPO Paradigms. From Table 4, we can infer that directly applying GRPO to the original models is not feasible. Therefore, in this part, we start with the model obtained in Table 5, which involves SFT with different sources of CoT data. We then progressively incorporate different rewards for comparison: the

original binary accuracy reward in GRPO and the DPA reward proposed in this paper, to evaluate the effectiveness of each reward type. To ensure consistency, we utilize the same CoT prompt across all models. From Table 6, we can conclude that the design of the accuracy-based reward directly impacts the effectiveness of the reinforcement learning method. The performance of the original accuracy reward is inferior to the DPA reward proposed in this paper. This demonstrates that the reward design in reinforcement learning must accurately reflect the intended actions. In the context of the multiple-choice question task in this paper, DPA reward aligns most closely with the actual scoring rules. We further enhance the DPA-GRPO algorithm by integrating the hard cases mining method from Figure 4. This combined approach, HCM-GRPO, yields the top score of 64.74 on the InternVL3-2B-CoT baseline, demonstrating that hard cases mining is an effective strategy for boosting the upper limits of the model's performance. For the InternVL3-1B-CoT model, we re-evaluate the performance differences among GRPO, DPA-GRPO, and HCM-GRPO. The conclusions are consistent with those from the InternVL3-2B-CoT experiments, confirming that our proposed HCM-GRPO method is also effective on the InternVL3-1B-CoT model.

Different Types of Mining Cases in HCM-GRPO. To investigate the impact of different data augmentation strategies during our HCM-GRPO training process, we conduct a comprehensive ablation study. The core of this study focuses on the composition of the dataset used in the last 2 epochs of the training stage. All experimental setups share a common first stage: the model is initially trained for 3 epochs on the fully-supervised training set of 1044 multiple-choice samples under the DPA-GRPO. Subsequently, we continue training for an additional 2 epochs but vary the data composition to analyze its effect on final performance. We evaluate the four strategies in Table 7. The results provide clear insights into the effectiveness of our proposed data strategy. Taking InternVL3-2B-CoT as an example, the model achieves the highest accuracy of 64.74 when trained on a mixture of the original 1044 multiple-choice samples and the curated hard cases. This result outperforms all other configurations. Comparing this top-performing model to the control group, which includes 1044 multiple-choice data with random samples, we observe a substantial performance gain. This confirms that the improvement is not merely an effect of data augmentation but is specifically at-

Table 7: Ablation study on the composition of training data in the last 2 epochs of stage2. All models were initially trained on 1044 supervised samples for first 3 epochs and last 2 epochs with the specified data.

Last 2 Epochs Data Composition	Overall Score		
InternVL3-2B-CoT			
434 Hard Cases Only	58.76 (-1.07)		
610 Easy Cases Only	59.40 (-0.43)		
All 1044 Samples (DPA-GRPO)	59.83 (+0.0)		
All 1044 Samples + 434 Random Samples	60.90 (+1.07)		
All 1044 Samples + 434 Hard Cases (HCM-GRPO)	64.74 (+4.91)		

tributable to the strategic inclusion of hard cases that target the model's weaknesses. Furthermore, the experiments involving training on the whole dataset or subsets yield inferior results. Training exclusively on hard cases (score of 58.76) or easy cases (score of 59.40) led to lower scores. This suggests two key points: (1) focusing only on difficult examples may cause the model to overfit to these niche cases and forget the general data distribution, a phenomenon known as catastrophic forgetting; (2) reinforcing only what the model already knows is an inefficient strategy that fails to address its deficiencies. In conclusion, the optimal approach is to supplement the full supervised dataset with a targeted set of hard cases. This method allows the model to continuously refine its understanding of its weak points without losing its grasp of the overall data distribution, leading to the most robust and accurate performance.

5.4. Generalization to Public Datasets

Considering the composition of our image aesthetic dataset, where each instance comprises multiple generated images for the purpose of identifying physical space errors, further evaluation on other public datasets is conducted. These public datasets were chosen primarily to evaluate HCM-GRPO in real-world physical reasoning and multi-image collaborative understanding. We select RealWorldQA [45], MuirBench [46], and BLINK [47] for further evaluation.

The RealWorldQA [45] dataset comprises 765 instances from the real physical world,

Table 8: Generalization study on the public dataset RealWorldQA.

model	Overall Accuracy
InternVL3-2B	61.52
+SFT	62.57 (+1.05)
+SFT, +GRPO	62.83 (+1.31)
+SFT, +HCM-GRPO	64.14 (+2.62)

Table 9: Generalization study on the public dataset MuirBench.

model	Overall Accuracy
InternVL3-1B	29.48
+SFT	62.35 (+32.87)
+SFT, +GRPO	63.04 (+33.56)
+SFT, +HCM-GRPO	63.43 (+33.95)

with each instance consisting of a question, an image, and its corresponding answer. We partition the RealWorldQA dataset into training and testing sets at a 1:1 ratio. On the testing set, we evaluate the performance differences among various fine-tuning methods, including SFT, GRPO, and our proposed HCM-GRPO, applied to the InternVL3-2B model. As shown in the table 8, the InternVL3-2B model achieves a score of 61.52. Our proposed HCM-GRPO combined with SFT outperforms that of GRPO, demonstrating its effectiveness in enhancing the model's understanding of real-world physical spaces. For this application, HCM-GRPO is configured as the GRPO framework augmented with hard cases mining, excluding the DPA reward component due to the single option nature of the RealWorldQA dataset. This specific implementation, despite lacking complex fine-tuning stages such as answer-driven CoT data, still demonstrates a notable performance gain of 2.62 points relative to the baseline model.

MuirBench [46] is a benchmark containing 11,264 images and 2,600 multiple-choice questions, providing robust evaluation on 12 multi-image understanding tasks. We partition the data from all subtasks within the MuirBench dataset into a 1:1 split for

training and testing, following the same experimental protocol as with RealWorldQA. Since some samples in the dataset contain a large number of images, which may lead to excessive GPU memory consumption during training, we chose InternVL3-1B as our baseline for validation. We then evaluate and compare the performance of the baseline against versions fine-tuned with SFT, GRPO, and our proposed HCM-GRPO on the newly created testing split. The results in Table 9 reveal a dramatic performance boost from SFT, suggesting that the validation data is highly in-distribution. This consequently limits the potential gains from subsequent RL training, as evidenced by the modest improvement from GRPO. Even under these conditions, our HCM-GRPO method demonstrates its effectiveness by delivering the highest performance of 63.43. The BLINK dataset consists of 14 classic computer vision tasks, ranging from lowlevel pattern matching to mid-level reasoning and extending to high-level visual understanding. This benchmark contains 3.8K samples, in which questions may contain multiple images. Since the test set of the BLINK dataset is unlabeled, we conduct our experiments on the validation set with InternVL3-1B and InternVL3-2B. The results in Table 10 demonstrate the effectiveness of our proposed HCM-GRPO on the BLINK dataset. Both GRPO and HCM-GRPO provide better performances for the InternVL3-1B and InternVL3-2B models. The combination of SFT and HCM-GRPO proves most effective, boosting the accuracy of InternVL3-2B to 49.10 and showcasing a substantial improvement of 8.92 over the base model.

6. Conclusion

In this work, we address the challenges of image screening with MLLMs by proposing a comprehensive solution that includes a novel dataset and an advanced training methodology. Our dataset evaluates image aesthetic reasoning ability across four critical dimensions, while our method leverages CoT data followed by HCM-GRPO reinforcement learning to significantly enhance performance. Notably, this task is highly challenging, as even leading closed-source MLLMs, such as GPT40 and Qwen-VL-Max, perform poorly at the level of random guessing. In contrast, our approach

Table 10: Generalization study on the public dataset BLINK.

model	Overall Accuracy
InternVL3-1B	33.30
+SFT	35.78 (+2.48)
+SFT, +GRPO	36.79 (+3.49)
+SFT, +HCM-GRPO	38.15 (+4.85)
InternVL3-2B	40.18
+SFT	45.15 (+4.97)
+SFT, +GRPO	47.97 (+7.79)
+SFT, +HCM-GRPO	49.10 (+8.92)

achieves superior results with a much smaller model, demonstrating the effectiveness of combining CoT data with reinforcement learning and the advantages of HCM-GRPO over the original GRPO. We believe these efforts will pave the way for more robust and reliable solutions in image aesthetic reasoning. Despite these achievements, some limitations still remain.

- Our model demonstrates good performance in recognizing appearance deformation and extension rationality, but it still struggles with placement layout as well as the physical shadow. Future work will focus on enriching the CoT data with high-quality examples from different dimensions. This enhancement is expected to provide a stronger foundation for the reinforcement learning phase, further improving the model's reasoning capabilities in complex scenarios.
- Beyond generating higher-quality CoT data to target model weaknesses, we aim to achieve knowledge transfer in an unsupervised manner. In this paper, we do not extensively utilize the exploration split of our dataset. Consequently, a key direction for future work is to focus on enabling knowledge transfer for image screening using large volumes of unsupervised data. The ultimate goal is to allow existing MLLMs to automatically acquire domain-specific knowledge.

Appendix A. More Benchmark Examples

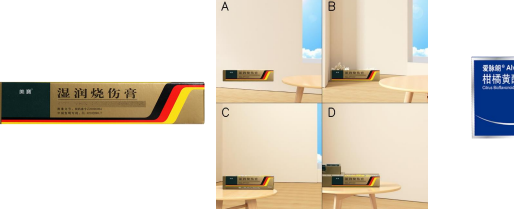
We present some samples from the dataset here. Figure A.5 shows some original images along with their corresponding generated images. In Figure A.6, we illustrate the reasoning process of the HCM-GRPO-2B model, with key words in the reasoning process highlighted in red and the decisions made by the model marked in blue.

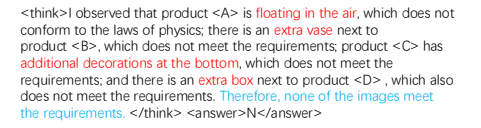


Figure A.5: Samples from the constructed dataset.

Appendix B. Prompt Template

We present the prompt here. There are two types of prompts. One type directly asks the model to output an answer, such as A, B, C, D, or N. The other type follows the GRPO thinking format, outputting the chains of thought process and the final answer. In all of our experiments, we use the following two types of prompts: CoT Format (highlighted in red) and Direct Format (highlighted in blue).







< have additional decorations, which do not match the original image; the shape of product < B is consistent with the original image, and the lighting and shadow layout is reasonable; product < C> is placed on a laptop, which does not match the original image; the edges of product <D> have additional decorations, which do not match the original image; the edges of product <D> have additional decorations, which do not match the original image. Therefore, the final choice is .

Figure A.6: Presentation of the reasoning process.

Prompt:

You are an expert in product operations review and possess significant artistic talent, excelling at creating product images.

Task

I have created four product images for a product, labeled A, B, C, and D. I need your help to select the one that meets the requirements.

Requirements

- 1. The image must not contain any items other than those in the original product image. Any changes to the product (including appearance, shape, quantity, etc.) will render the image unacceptable, regardless of how visually appealing it may be. This is the most fundamental requirement.
- 2. Lighting, composition, and other elements should adhere to physical laws, avoiding issues such as incorrect shadows, floating products, or other unreasonable phenomena.

Output Format

1. Only one answer can be provided. If none of the images meet the requirements, you should output 'N'. If multiple images meet the requirements, choose the one that best aligns with aesthetic standards.

- 2. Provide your thought process by sequentially observing each image to check for any product changes and evaluate the lighting and layout. Ultimately, select the most appropriate image. Follow this format: '<think>I observed <A> XXX, XXX, <C> XXX, <D> XXX, so I ultimately chose .</think><answer>B
- 3. Analyze each image (A, B, C, D) from multiple dimensions to determine its reasonableness, then provide the answer you believe is the most suitable. (CoT Format)
- 2. Provide only the final numbered answer, following this format: A, B, C, D, or N. (Direct Format)

Input

Original image: <image>
Generated images: <image>

Output

References

- [1] J. Zhu, W. Wang, Z. Chen, Z. Liu, S. Ye, L. Gu, Y. Duan, H. Tian, W. Su, J. Shao, et al., Internvl3: Exploring advanced training and test-time recipes for open-source multimodal models, arXiv preprint arXiv:2504.10479 (2025).
- [2] S. Bai, K. Chen, X. Liu, J. Wang, W. Ge, S. Song, K. Dang, P. Wang, S. Wang, J. Tang, et al., Qwen2. 5-vl technical report, arXiv preprint arXiv:2502.13923 (2025).
- [3] S. Lu, Y. Li, Q.-G. Chen, Z. Xu, W. Luo, K. Zhang, H.-J. Ye, Ovis: Structural embedding alignment for multimodal large language model, arXiv preprint arXiv:2405.20797 (2024).
- [4] H. Cai, Y. Yang, W. Hu, Mm-iq: Benchmarking human-like abstraction and reasoning in multimodal models, arXiv preprint arXiv:2502.00698 (2025).
- [5] Z. Yang, J. Tang, Z. Li, P. Wang, J. Wan, H. Zhong, X. Liu, M. Yang, P. Wang, Y. Liu, et al., Cc-ocr: A comprehensive and challenging ocr benchmark for evaluating large multimodal models in literacy, arXiv preprint arXiv:2412.02210 (2024).
- [6] Z. Cheng, Q. Chen, J. Zhang, H. Fei, X. Feng, W. Che, M. Li, L. Qin, Comt: A novel benchmark for chain of multi-modal thought on large vision-language models, in: Proceedings of the AAAI Conference on Artificial Intelligence, Vol. 39, 2025, pp. 23678–23686.
- [7] Z. Liu, Z. Sun, Y. Zang, X. Dong, Y. Cao, H. Duan, D. Lin, J. Wang, Visual-rft: Visual reinforcement fine-tuning, arXiv preprint arXiv:2503.01785 (2025).
- [8] W. Wang, Z. Gao, L. Chen, Z. Chen, J. Zhu, X. Zhao, Y. Liu, Y. Cao, S. Ye, X. Zhu, et al., Visualprm: An effective process reward model for multimodal reasoning, arXiv preprint arXiv:2503.10291 (2025).
- [9] H. Wang, C. Qu, Z. Huang, W. Chu, F. Lin, W. Chen, Vl-rethinker: Incentivizing self-reflection of vision-language models with reinforcement learning, arXiv preprint arXiv:2504.08837 (2025).

- [10] X. Chen, Z. Wu, X. Liu, Z. Pan, W. Liu, Z. Xie, X. Yu, C. Ruan, Janus-pro: Unified multimodal understanding and generation with data and model scaling, arXiv preprint arXiv:2501.17811 (2025).
- [11] Q. Sun, Y. Cui, X. Zhang, F. Zhang, Q. Yu, Y. Wang, Y. Rao, J. Liu, T. Huang, X. Wang, Generative multimodal models are in-context learners, in: Proceedings of the IEEE/CVF Conference on Computer Vision and Pattern Recognition, 2024, pp. 14398–14409.
- [12] K. Tian, Y. Jiang, Z. Yuan, B. Peng, L. Wang, Visual autoregressive modeling: Scalable image generation via next-scale prediction, Advances in neural information processing systems 37 (2024) 84839–84865.
- [13] Z. Huang, S. Zhuang, C. Fu, B. Yang, Y. Zhang, C. Sun, Z. Zhang, Y. Wang, C. Li, Z.-J. Zha, Wegen: A unified model for interactive multimodal generation as we chat, arXiv preprint arXiv:2503.01115 (2025).
- [14] J. Ho, A. Jain, P. Abbeel, Denoising diffusion probabilistic models, Advances in neural information processing systems 33 (2020) 6840–6851.
- [15] R. Rombach, A. Blattmann, D. Lorenz, P. Esser, B. Ommer, High-resolution image synthesis with latent diffusion models, in: Proceedings of the IEEE/CVF conference on computer vision and pattern recognition, 2022, pp. 10684–10695.
- [16] D. Podell, Z. English, K. Lacey, A. Blattmann, T. Dockhorn, J. Müller, J. Penna, R. Rombach, Sdxl: Improving latent diffusion models for high-resolution image synthesis, arXiv preprint arXiv:2307.01952 (2023).
- [17] W. Peebles, S. Xie, Scalable diffusion models with transformers, in: Proceedings of the IEEE/CVF international conference on computer vision, 2023, pp. 4195– 4205.
- [18] H. Ye, J. Zhang, S. Liu, X. Han, W. Yang, Ip-adapter: Text compatible image prompt adapter for text-to-image diffusion models, arXiv preprint arXiv:2308.06721 (2023).

- [19] H. Zhang, Z. Duan, X. Wang, Y. Chen, Y. Zhao, Y. Zhang, Nexus-gen: A unified model for image understanding, generation, and editing, arXiv preprint arXiv:2504.21356 (2025).
- [20] L. Zhang, A. Rao, M. Agrawala, Adding conditional control to text-to-image diffusion models, in: Proceedings of the IEEE/CVF international conference on computer vision, 2023, pp. 3836–3847.
- [21] Z. Tan, S. Liu, X. Yang, Q. Xue, X. Wang, Ominicontrol: Minimal and universal control for diffusion transformer, arXiv preprint arXiv:2411.15098 (2024).
- [22] H. Zhu, Y. Zhou, R. Yao, G. Wang, Y. Yang, Learning image aesthetic subjectivity from attribute-aware relational reasoning network, Pattern Recognition Letters 155 (2022) 84–91.
- [23] L. Li, Y. Huang, J. Wu, Y. Yang, Y. Li, Y. Guo, G. Shi, Theme-aware visual attribute reasoning for image aesthetics assessment, IEEE Transactions on Circuits and Systems for Video Technology 33 (9) (2023) 4798–4811.
- [24] Z. Zhou, Q. Wang, B. Lin, Y. Su, R. Chen, X. Tao, A. Zheng, L. Yuan, P. Wan, D. Zhang, Uniaa: A unified multi-modal image aesthetic assessment baseline and benchmark, arXiv preprint arXiv:2404.09619 (2024).
- [25] P. Zheng, D. Gao, D.-P. Fan, L. Liu, J. Laaksonen, W. Ouyang, N. Sebe, Bilateral reference for high-resolution dichotomous image segmentation, CAAI Artificial Intelligence Research (2024).
- [26] B. F. Labs, Flux, https://github.com/black-forest-labs/flux (2024).
- [27] Z. Shao, P. Wang, Q. Zhu, R. Xu, J. Song, X. Bi, H. Zhang, M. Zhang, Y. Li, Y. Wu, et al., Deepseekmath: Pushing the limits of mathematical reasoning in open language models, arXiv preprint arXiv:2402.03300 (2024).
- [28] D. Guo, D. Yang, H. Zhang, J. Song, R. Zhang, R. Xu, Q. Zhu, S. Ma, P. Wang, X. Bi, et al., Deepseek-r1: Incentivizing reasoning capability in Ilms via reinforcement learning, arXiv preprint arXiv:2501.12948 (2025).

- [29] Z. Chen, W. Wang, H. Tian, S. Ye, Z. Gao, E. Cui, W. Tong, K. Hu, J. Luo, Z. Ma, et al., How far are we to gpt-4v? closing the gap to commercial multimodal models with open-source suites, Science China Information Sciences 67 (12) (2024) 220101.
- [30] W. Wang, Z. Chen, W. Wang, Y. Cao, Y. Liu, Z. Gao, J. Zhu, X. Zhu, L. Lu, Y. Qiao, et al., Enhancing the reasoning ability of multimodal large language models via mixed preference optimization, arXiv preprint arXiv:2411.10442 (2024).
- [31] W. Hong, W. Yu, X. Gu, G. Wang, G. Gan, H. Tang, J. Cheng, J. Qi, J. Ji, L. Pan, et al., Glm-4.1 v-thinking: Towards versatile multimodal reasoning with scalable reinforcement learning, arXiv e-prints (2025) arXiv–2507.
- [32] B. Li, Z. Lin, W. Peng, J. d. D. Nyandwi, D. Jiang, Z. Ma, S. Khanuja, R. Krishna, G. Neubig, D. Ramanan, Naturalbench: Evaluating vision-language models on natural adversarial samples, arXiv preprint arXiv:2410.14669 (2024).
- [33] C.-H. Yeh, C. Wang, S. Tong, T.-Y. Cheng, R. Wang, T. Chu, Y. Zhai, Y. Chen, S. Gao, Y. Ma, Seeing from another perspective: Evaluating multi-view understanding in mllms, arXiv preprint arXiv:2504.15280 (2025).
- [34] Q. Yu, Z. Zhang, R. Zhu, Y. Yuan, X. Zuo, Y. Yue, T. Fan, G. Liu, L. Liu, X. Liu, et al., Dapo: An open-source llm reinforcement learning system at scale, 2025, URL https://arxiv.org/abs/2503.14476.
- [35] Y. Yuan, Q. Yu, X. Zuo, R. Zhu, W. Xu, J. Chen, C. Wang, T. Fan, Z. Du, X. Wei, et al., Vapo: Efficient and reliable reinforcement learning for advanced reasoning tasks, arXiv preprint arXiv:2504.05118 (2025).
- [36] K. Zhang, Y. Hong, J. Bao, H. Jiang, Y. Song, D. Hong, H. Xiong, Gvpo: Group variance policy optimization for large language model post-training, arXiv preprint arXiv:2504.19599 (2025).

- [37] C. Zheng, S. Liu, M. Li, X.-H. Chen, B. Yu, C. Gao, K. Dang, Y. Liu, R. Men, A. Yang, et al., Group sequence policy optimization, arXiv preprint arXiv:2507.18071 (2025).
- [38] Y. Wang, Z. Li, Y. Zang, C. Wang, Q. Lu, C. Jin, J. Wang, Unified multimodal chain-of-thought reward model through reinforcement fine-tuning, arXiv preprint arXiv:2505.03318 (2025).
- [39] J. Zhang, J. Huang, H. Yao, S. Liu, X. Zhang, S. Lu, D. Tao, R1-vl: Learning to reason with multimodal large language models via step-wise group relative policy optimization, arXiv preprint arXiv:2503.12937 (2025).
- [40] Alibaba Cloud, Qwen-vl-max alibaba cloud, https://www.aliyun.com.
- [41] W. Wang, Z. Gao, L. Gu, H. Pu, L. Cui, X. Wei, Z. Liu, L. Jing, S. Ye, J. Shao, et al., Internvl3. 5: Advancing open-source multimodal models in versatility, reasoning, and efficiency, arXiv preprint arXiv:2508.18265 (2025).
- [42] OpenAI, Gpt-4o openai, https://openai.com.
- [43] Alibaba Cloud, Qwen-vl-plus alibaba cloud, https://www.aliyun.com.
- [44] Y. Zhao, J. Huang, J. Hu, X. Wang, Y. Mao, D. Zhang, Z. Jiang, Z. Wu, B. Ai, A. Wang, W. Zhou, Y. Chen, Swift:a scalable lightweight infrastructure for fine-tuning (2024). arXiv:2408.05517.
 URL https://arxiv.org/abs/2408.05517
- [45] X.AI Corp, Grok-1.5 vision preview: Connecting the digital and physical worlds with our first multimodal model, https://x.ai/blog/grok-1.5v.
- [46] F. Wang, X. Fu, J. Y. Huang, Z. Li, Q. Liu, X. Liu, M. D. Ma, N. Xu, W. Zhou, K. Zhang, et al., Muirbench: A comprehensive benchmark for robust multi-image understanding, arXiv preprint arXiv:2406.09411 (2024).
- [47] X. Fu, Y. Hu, B. Li, Y. Feng, H. Wang, X. Lin, D. Roth, N. A. Smith, W.-C. Ma, R. Krishna, Blink: Multimodal large language models can see but not perceive, in: European Conference on Computer Vision, Springer, 2024, pp. 148–166.